NUCL SCI TECH (2021) 32:46
https://doi.org/10.1007/s41365-021-00884-0

Searching for single-particle resonances with the Green's function method

Ya-Tian Wang[1] · **Ting-Ting Sun**[1]

Received: 14 January 2021 / Revised: 17 March 2021 / Accepted: 18 March 2021 / Published online: 8 May 2021

Abstract Single-particle resonances in the continuum are crucial for studies of exotic nuclei. In this study, the Green's function approach is employed to search for single-particle resonances based on the relativistic-mean-field model. Taking ^{120}Sn as an example, we identify single-particle resonances and determine the energies and widths directly by probing the extrema of the Green's functions. In contrast to the results found by exploring for the extremum of the density of states proposed in our recent study [Chin. Phys. C, 44:084105 (2020)], which has proven to be very successful, the same resonances as well as very close energies and widths are obtained. By comparing the Green's functions plotted in different coordinate space sizes, we also found that the results very slightly depend on the space size. These findings demonstrate that the approach by exploring for the extremum of the Green's function is also very reliable and effective for identifying resonant states, regardless of whether they are wide or narrow.

Keywords Single-particle resonances · Extrema of Green's functions · Relativistic-mean-field theory

This work was supported by the National Natural Science Foundation of China (No. U2032141), the Natural Science Foundation of Henan Province (No. 202300410479 and No. 202300410480), the Foundation of Fundamental Research for Young Teachers of Zhengzhou University (No. JC202041041), and the Physics Research and Development Program of Zhengzhou University (No. 32410217).

✉ Ting-Ting Sun
ttsunphy@zzu.edu.cn

[1] School of Physics and Microelectronics, Zhengzhou University, Zhengzhou 450001, China

1 Introduction

Recently, explorations for single-particle resonances are attracting increasing attention because of their significant role in studies of exotic nuclei. Many exotic phenomena such as halos [1], deformed halos [2], and giant halos [3–5] are explained by the occupations of valence neutrons in the continuum. For example, giant halos predicted in neutron-rich Zr and Ca isotopes are caused by valence neutrons scattered to the continuum and occupying p orbitals [3, 4], and the possible deformed halos in ^{40,42}Mg and ^{22}C are mainly caused by the occupations of single-particle states around the Fermi surface [6–8]. Numerous studies have shown that, in weakly bound exotic nuclei with very small gaps, between the Fermi surface and the continuum threshold, the valence nucleons can be scattered to the continuum effortlessly by pairing correlations. Halos can be formed if the valence nucleons occupy an orbit with a small angular momentum l, which can contribute a large radius [9, 10].

To explore single-particle resonances, researchers have developed a series of approaches. One technique starts from scattering theory, such as K-matrix theory [11], S-matrix theory [12, 13], R-matrix theory [14, 15], the Jost function approach [16, 17], and the scattering phase shift method [18, 19]. Meanwhile, approaches for bound states are also widely used; these include the real stabilization method [20, 21], the complex scaling method [22–25], the analytical continuation of the coupling constant method [26, 27], the complex momentum representation method [28, 29], and the complex-scaled Green's function method [30].

The Green's function approach [31, 32], which has wide applications in various fields of physics [33, 34], has also

been demonstrated to be very effective for studying the continuum and single-particle resonant states. Owing to its advantages, such as its being able to handle bound states and the continuum uniformly by using the density of states (DOS) tool, the resonance energies and widths can be determined easily, the asymptotic behavior of the spatial extended density in weakly bound nuclei can be properly described, and, most importantly, it can be combined with different nuclear models very conveniently. The Green's function method has yielded significant achievements in nuclear physics in investigating the effects of the continuum on the properties of atomic nuclei. For example, to describe the continuum exactly in exotic nuclei near the drip line and study the possible effects of the continuum on the properties of the ground state, Zhang et al. developed the self-consistent continuum Skyrme Hartree–Fock–Bogoliubov (HFB) theory [35, 36], based on which a series of research projects have been conducted. These include establishment of the energies and wave functions for single-particle canonical bound and resonant states with different space sizes [37], study of the possible impacts of mean field and pairing on the resonances [38, 39], and the extension to the odd-*A* systems by including the blocking effect [40]. To explore the contribution of the continuous spectrum to nuclear collective excitations, Matsuo applied the HFB Green's function [41] to the quasiparticle random-phase approximation [42, 43], enabling further study of the collective excitations coupled to the continuum [44–47], microscopic structures of monopole pair vibrational modes and associated two-neutron transfer amplitudes [48], and neutron capture reactions [49].

Given the great successes that the Green's function method achieved in the nonrelativistic framework, it is naturally applied in covariant density functional theory [50–52], which has been demonstrated to be a powerful tool in researching various nuclear systems and properties, such as superheavy nuclei [53–55], pseudospin symmetry [56–58], hypernuclei [59–61], and neutron stars [62, 63]. In Refs. [64, 65], the relativistic continuum random-phase approximation theory is developed by adopting the Green's function of the Dirac equation [31] to investigate collective excitations. In Ref. [66], we introduced the Green's function approach to the relativistic-mean-field (RMF) model and studied single-particle resonances for the first time. Later, this approach was further extended to studies of single-particle resonances of protons [67], hyperons [68], and those in deformed nuclei with a quadrupole-deformed Woods–Saxon potential [69]. In addition, the pseudospin symmetries hidden in resonant states were also investigated by applying the Green's function method [70]. In Ref. [71], to study the halo structures in neutron-rich nuclei, we further included the pairing correlation and introduced the Green's function approach to the continuum relativistic Hartree–Bogoliubov theory.

In our previous studies of single-particle resonant states [66–68], the resonant states are determined by comparing the DOS of particles in the mean field to those for free particles. In this framework, resonance energies and widths are simply determined as the position and full width at half-maximum of the resonant peak, respectively. With this method, one can describe narrow resonances very well, but the accuracy is poor for wide ones. Therefore, in our recent studies [69, 72], we proposed an effective and direct way to identify the resonant states by exploring for the extremum of the DOS. The exact energies and widths for the resonant states in all types can be obtained, whether for wide or narrow resonant states. However, the DOS in the calculations are approximate ones because they are calculated in a finite space size. In this work, we will directly analyze Green's functions and search for their poles or extrema to determine the resonant states.

The paper is organized as follows: The RMF model formulated with Green's functions is briefly presented in Sect. 2. Numerical details are given in Sect. 3. After the results and discussion are presented in Sect. 4, a brief summary and perspectives are given in Sect. 5.

2 Theoretical framework

In the RMF model, neutrons and protons are described as Dirac particles moving in a mean-field potential characterized by scalar S and vector V potentials. The Dirac equation for a nucleon with mass M is as follows:

$$[\boldsymbol{\alpha}\cdot\boldsymbol{p}+V(\boldsymbol{r})+\beta(M+S(\boldsymbol{r}))]\psi_n(\boldsymbol{r})=\varepsilon_n\psi_n(\boldsymbol{r}), \tag{1}$$

where $\boldsymbol{\alpha}$ and β are Dirac matrices.

Various methods have been used to solve the Dirac equation. These include the shooting method [10], the Green's function method [66], and the finite element method [73], which are performed in the coordinate space, as well as those in the harmonic oscillator basis [74] or Woods–Saxon basis [75]. When introducing the Green's function method to mean-field density functionals, the densities and single-particle spectrum can be determined directly by the Green's functions [35, 36, 40, 66]. Following the definition of the single-particle Green's function,

$$[\varepsilon-\hat{h}(\boldsymbol{r})]\mathcal{G}(\boldsymbol{r},\boldsymbol{r}';\varepsilon)=\delta(\boldsymbol{r}-\boldsymbol{r}'), \tag{2}$$

a relativistic Green's function $\mathcal{G}(\boldsymbol{r},\boldsymbol{r}';\varepsilon)$ for the Dirac equation can be constructed at arbitrary single-particle energies ε when $\hat{h}(\boldsymbol{r})$ is chosen as the Dirac Hamiltonian. Taking a complete set of solutions of the Dirac equation,

including the eigenstates $\psi_n(\boldsymbol{r})$ and eigenvalues ε_n, we can write the Green's function in Eq. (2) as

$$\mathcal{G}(\boldsymbol{r},\boldsymbol{r}';\varepsilon)=\sum_n \frac{\psi_n(\boldsymbol{r})\psi_n^\dagger(\boldsymbol{r}')}{\varepsilon-\varepsilon_n}. \tag{3}$$

With the single-particle energy ε approaching the energy ε_n, the absolute value of $\mathcal{G}(\boldsymbol{r},\boldsymbol{r}';\varepsilon)$ will increase significantly and reach the extremum. Therefore, one can determine the single-particle energies ε_n by calculating different Green's functions at various energies ε and search for the extremum. For resonant states with resonant energies E and widths Γ, one can write their energies as $\varepsilon_n = E - i\Gamma/2$. Correspondingly, the energies ε in Eqs. (2) and (3) are complex: $\varepsilon = \varepsilon_r + i\varepsilon_i$ with ε_r and ε_i being the real and imaginary parts of the energy, respectively.

Because the Dirac spinor $\psi_n(\boldsymbol{r})$ has upper and lower components, the corresponding Green's function has the form of a 2×2 matrix,

$$\mathcal{G}(\boldsymbol{r},\boldsymbol{r}';\varepsilon)=\begin{pmatrix}\mathcal{G}^{(11)}(\boldsymbol{r},\boldsymbol{r}';\varepsilon) & \mathcal{G}^{(12)}(\boldsymbol{r},\boldsymbol{r}';\varepsilon)\\ \mathcal{G}^{(21)}(\boldsymbol{r},\boldsymbol{r}';\varepsilon) & \mathcal{G}^{(22)}(\boldsymbol{r},\boldsymbol{r}';\varepsilon)\end{pmatrix}. \tag{4}$$

With spherical symmetry, one can expand the Green's function as

$$\mathcal{G}(\boldsymbol{r},\boldsymbol{r}';\varepsilon)=\sum_{\kappa m} Y_{\kappa m}(\theta,\phi)\frac{\mathcal{G}_\kappa(r,r';\varepsilon)}{rr'}Y^*_{\kappa m}(\theta',\phi'), \tag{5}$$

where $\mathcal{G}_\kappa(r,r';\varepsilon)$ is the radial part, $Y_{\kappa m}(\theta,\phi)$ is the spin spherical harmonic, and the quantum number $\kappa = (-1)^{j+l+1/2}(j+1/2)$ labels different "channels".

For a given single-particle energy ε and quantum number κ, we can construct the radial Green's function $\mathcal{G}_\kappa(r,r';\varepsilon)$ as [31]

$$\begin{aligned}\mathcal{G}_\kappa(r,r';\varepsilon)=\frac{1}{W_\kappa(\varepsilon)}\Big[&\theta(r-r')\phi_\kappa^{(2)}(r,\varepsilon)\phi_\kappa^{(1)\dagger}(r',\varepsilon)\\ &+\theta(r'-r)\phi_\kappa^{(1)}(r,\varepsilon)\phi_\kappa^{(2)\dagger}(r',\varepsilon)\Big],\end{aligned} \tag{6}$$

with $\phi_\kappa^{(1)}(r,\varepsilon)$ and $\phi_\kappa^{(2)}(r,\varepsilon)$ being two Dirac spinors given by

$$\begin{aligned}\phi_\kappa^{(1)}(r,\varepsilon)&=\begin{pmatrix}g_\kappa^{(1)}(r,\varepsilon)\\ f_\kappa^{(1)}(r,\varepsilon)\end{pmatrix},\\ \phi_\kappa^{(2)}(r,\varepsilon)&=\begin{pmatrix}g_\kappa^{(2)}(r,\varepsilon)\\ f_\kappa^{(2)}(r,\varepsilon)\end{pmatrix},\end{aligned} \tag{7}$$

which are linearly independent and obtained by solving the Runge–Kutta integrals in the full coordinate r space starting, respectively, from the asymptotic behaviors at $r\to 0$ and $r\to\infty$; $\theta(r-r')$ is a step function; and $W_\kappa(\varepsilon)$ is the Wronskian function,

$$W_\kappa(\varepsilon)=g_\kappa^{(1)}(r,\varepsilon)f_\kappa^{(2)}(r,\varepsilon)-g_\kappa^{(2)}(r,\varepsilon)f_\kappa^{(1)}(r,\varepsilon), \tag{8}$$

which is independent of r. It can be checked that the constructed Green's function $\mathcal{G}_\kappa(r,r';\varepsilon)$ of Eq. (6) meets the definition Eq. (2) in the radial form.

In practical calculations, one will adopt the exact asymptotic behaviors of the Dirac spinors to construct Green's functions. As a result, weakly bound states around the Fermi surface as well as the resonances above the continuum threshold, which are essential for the unstable nuclei, can be addressed when calculating densities and single-particle spectra. At $r\to 0$, the asymptotic behavior of the Dirac spinor $\phi_\kappa^{(1)}(r,\varepsilon)$ satisfies

$$\phi_\kappa^{(1)}(r,\varepsilon)\longrightarrow r\begin{pmatrix}j_l(kr)\\ \dfrac{\kappa}{|\kappa|}\dfrac{\varepsilon-V-S}{k}j_{\tilde{l}}(kr)\end{pmatrix}, \tag{9}$$

where $k=\sqrt{(\varepsilon-V-S)(\varepsilon-V+S+2M)}$ is the single-particle momentum, the quantum number $\tilde{l}=l+(-1)^{j+l-1/2}$ denotes the angular momentum for the lower component of the Dirac spinor, and $j_l(kr)$ is the spherical Bessel function of the first kind, which satisfies

$$j_l(kr)\longrightarrow\frac{(kr)^l}{(2l+1)!!},\ \text{when } r\to 0. \tag{10}$$

At $r\to\infty$, the Dirac spinor $\phi_\kappa^{(2)}(r,\varepsilon)$ is oscillating outgoing for the continuum and exponentially decaying for the bound states, which can be represented uniformly as

$$\phi_\kappa^{(2)}(r,\varepsilon)\longrightarrow\begin{pmatrix}rkh_l^{(1)}(kr)\\ \dfrac{\kappa}{|\kappa|}\dfrac{rk^2}{\varepsilon+2M}h_{\tilde{l}}^{(1)}(kr)\end{pmatrix}, \tag{11}$$

where $k=\sqrt{\varepsilon(\varepsilon+2M)}$ and $h_l^{(1)}(kr)$ is the spherical Hankel function of the first kind.

3 Numerical details

In this work, the single-particle resonant states were studied by employing the Green's function method based on RMF theory, where the resonance energies E and widths Γ were obtained directly by probing the extrema of the Green's functions. To compare with the previous results obtained by using Green's functions calculations [66, 72], where the resonances were identified by probing the extremum of the DOS, $n_\kappa(\varepsilon)$, defined in a finite space size R_{box}, the same nucleus ^{120}Sn and density functional PK1 [76] were adopted.

The Green's functions and RMF equations were solved in the coordinate r space with a space size of $R_{\text{box}} = 20$ fm and a step of $\mathrm{d}\,r = 0.1$ fm. To check the dependence of

the obtained resonances on the space sizes, calculations with $R_{\rm box} = 25, 30$ fm were also performed. To search for the energy position corresponding to the poles of the Green's functions, the complex single-particle energies $\varepsilon = \varepsilon_r + i\varepsilon_i$ were scanned widely on the complex energy plane to calculate the Green's functions $\mathcal{G}(r, r; \varepsilon)$. The energy step was $\mathrm{d}\,\varepsilon = 1 \times 10^{-4}$ MeV for both the real ε_r and imaginary ε_i parts. With this scanning energy step, the accuracy of the obtained resonance energies and widths were up to 0.1 keV. In addition, the accuracy can be increased further once the scanning energy step $d\varepsilon$ is decreased.

4 Results and discussion

On the complex single-particle energy plane, single-particle resonances are located in the fourth quadrant, with the real energy being the resonance energy E and the imaginary energy being half of the resonance width $\Gamma/2$. According to Eq. (3), the single-particle energies $\varepsilon_n = E - i\Gamma/2$ of the resonant states also correspond to the extrema of the Green's functions $\mathcal{G}(r, r; \varepsilon)$. As a result, one can search for these poles or extrema to determine the locations of the resonant states by scanning the complex energies $\varepsilon = \varepsilon_r + i\varepsilon_i$ in the fourth quadrant and calculating the Green's functions $\mathcal{G}(r, r; \varepsilon)$.

In Fig. 1, taking the neutron single-particle resonant state $2f_{5/2}$ in ^{120}Sn as an example, we plot the Green's functions $\mathcal{G}(r, r; \varepsilon)$ at various scanned single-particle complex energies $\varepsilon = \varepsilon_r + i\varepsilon_i$. With the real energy ε_r varying from 0.8703 to 0.8707 MeV and the imaginary energy ε_i varying from -0.0324 to -0.0328 MeV, the height of the Green's function changes significantly. Comparing panels (a), (b), and (c) in the left column, we can see that the modulus of the Green's function $|\mathcal{G}^{(11)}|$ has a larger amplitude at a real energy $\varepsilon_r = 0.8705$MeV, as shown in panel (b). More specifically, the Green's function reaches its extremum at an imaginary energy $\varepsilon_i = -0.0326$MeV (plotted by the red line). All these analyses indicate that the Green's function reaches its extremum at an energy of $\varepsilon = 0.8705 - i0.0326$ MeV. In the same way, we show the moduli of the Green's functions for the "22" component $|\mathcal{G}^{(22)}|$ in the right column, which are determined by the small component of the Dirac spinor. The amplitudes are much lower than those in the left column. However, the Green's function reaches its maximum amplitude at the same energy $\varepsilon = 0.8705 - i0.0326$ MeV. Therefore, we can conclude that $\varepsilon = 0.8705 - i0.0326$ MeV corresponds to the energy of the single-particle resonant state $2f_{5/2}$ in ^{120}Sn, which is almost the same value as the result obtained by exploring for the extremum of the DOS [72] with a difference of 0.1 keV for the width.

To be more intuitive, one can integrate the Green's function $\mathcal{G}(r, r; \varepsilon)$ over coordinate r and compare the integral values at different scanning single-particle energies ε.

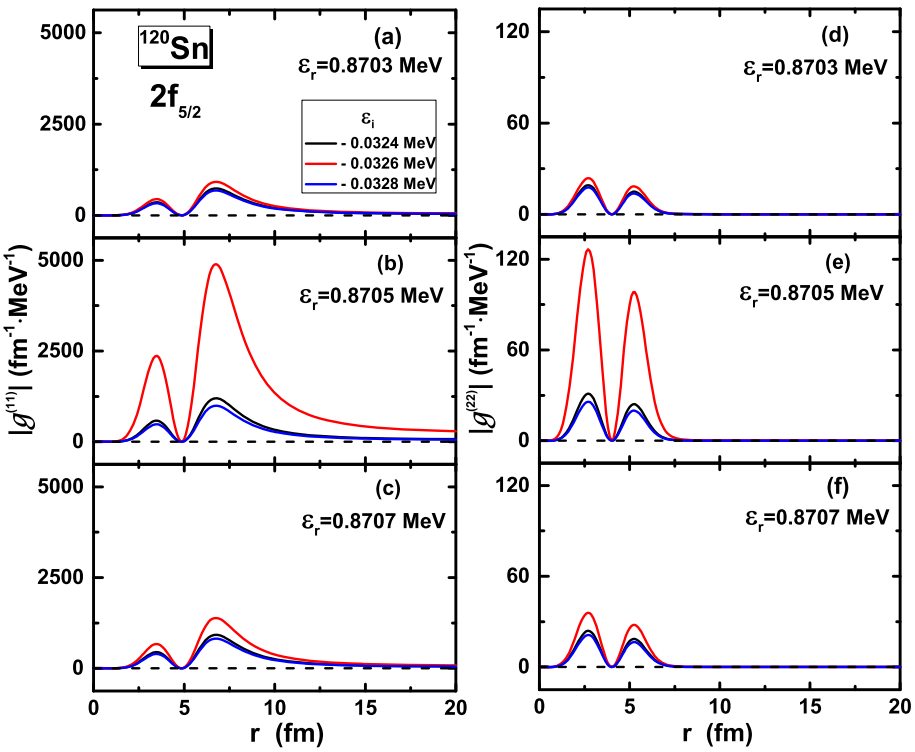

Fig. 1 (Color online) Green's functions $\mathcal{G}(r, r; \varepsilon)$ at different complex energies $\varepsilon = \varepsilon_r + i\varepsilon_i$ plotted as a function of coordinate r for the resonant state $2f_{5/2}$ in ^{120}Sn. The left and right columns are, respectively, the moduli of "11" and "22" components of Green's functions $|\mathcal{G}^{(11)}|$ and $|\mathcal{G}^{(22)}|$. The complex energy ε is scanned widely, and the results with the real energies $\varepsilon_r = 0.8703$, 0.8705, and 0.8707 MeV, and imaginary energies $\varepsilon_i = -0.0324$, -0.0326, and -0.0328 MeV are shown

The integral function $G_\kappa(\varepsilon)$ for each partial wave κ at energy ε can be written as

$$G_\kappa(\varepsilon) = \int \mathrm{d}\, r[|\mathcal{G}_\kappa^{(11)}(r,r;\varepsilon)| + |\mathcal{G}_\kappa^{(22)}(r,r;\varepsilon)|], \qquad (12)$$

where $|\mathcal{G}_\kappa^{(11)}(r,r;\varepsilon)|$ and $|\mathcal{G}_\kappa^{(22)}(r,r;\varepsilon)|$, respectively, correspond to the moduli of the "11" and "22" matrix elements of the Green's functions, as shown in Eq. (4). A sharp peak should be observed for the integral function $G_\kappa(\varepsilon)$ at the energy where the Green's function reaches its extremum. In Fig. 2, the result for the single-particle resonant state $2f_{5/2}$ in ^{120}Sn is plotted on the complex energy plane. A peak with an extremum located at $\varepsilon_r = 0.8705$ MeV and $\varepsilon_i = -0.0326$ MeV is observed, indicating that the energy of the resonant state $2f_{5/2}$ is $\varepsilon_n = 0.8705 - i0.0326$ MeV, which is the same as the result obtained in Fig. 1.

To check the universality of this approach, the same analysis was performed for a relatively wide single-particle resonant state $2g_{9/2}$ in Fig. 3. Similarly, a sharp peak is identified with the extremum located at $\varepsilon_r = 5.4428$ MeV and $\varepsilon_i = -1.6948$ MeV, indicating that the energy of the resonant state $2g_{9/2}$ is $\varepsilon_n = 5.4428 - i1.6948$ MeV. However, compared with the narrow resonant state $2f_{5/2}$, the peak of the wide resonant state $2g_{9/2}$ is much sharper, which can be explained by the greater integral values $G_\kappa(\varepsilon)$ for the wide resonant states caused by the extended distributions of Green's functions. From Figs. 2 and 3, we can conclude that it is very direct and effective to search for the single-particle resonant states and determine the energies and widths for both narrow and wide resonances by searching for the extrema of the Green's functions.

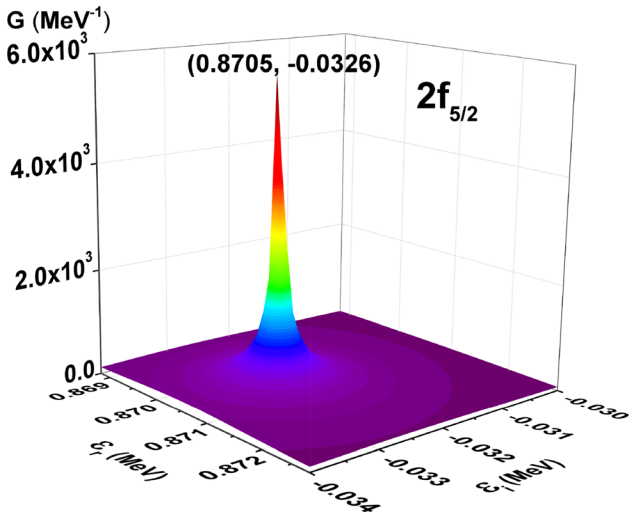

Fig. 2 (Color online) Integral function $G_\kappa(\varepsilon)$ distributed on the complex energy plane for the resonant state $2f_{5/2}$ in ^{120}Sn

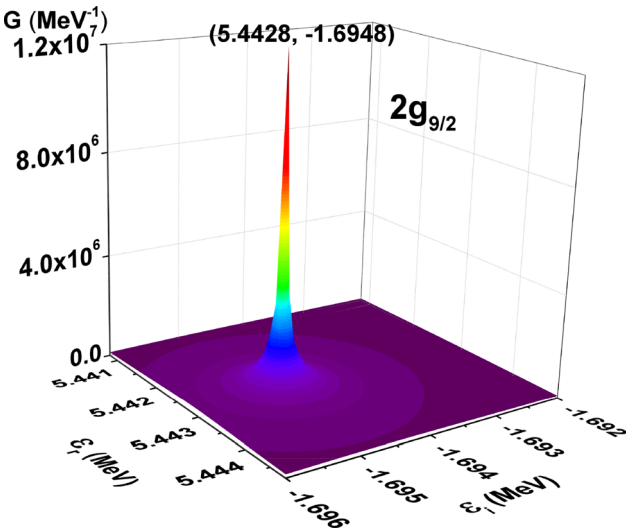

Fig. 3 (Color online) Integral function $G_\kappa(\varepsilon)$ distributed on the complex energy plane for the resonant state $2g_{9/2}$ in ^{120}Sn

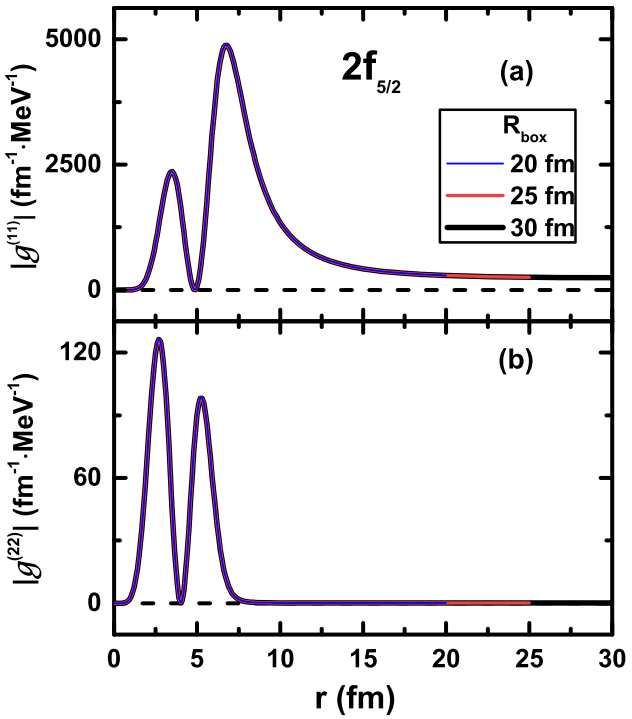

Fig. 4 (Color online) Green's functions $\mathcal{G}(r,r;\varepsilon)$ for the resonant state $2f_{5/2}$ in ^{120}Sn at the resonant energy $\varepsilon = E - i\Gamma/2$ calculated with space sizes R_{box} =20, 25, and 30 fm

In Fig. 4, the dependence of the Green's functions on the coordinate space sizes R_{box} is checked by taking the resonant state $2f_{5/2}$ as an example and plotting $|\mathcal{G}^{(11)}(r,r;\varepsilon)|$ and $|\mathcal{G}^{(22)}(r,r;\varepsilon)|$ with $R_{\text{box}} = 20$, 25, and 30 fm, respectively. Obviously, we can see that exactly the same distributions for both the "11" and "22" components are obtained, indicating that the Green's function method

depends slightly on the space sizes, which is consistent with the conclusions obtained by analyzing the density distributions $\rho_\kappa(r,\varepsilon)$ plotted in different space sizes [72].

In Table 1, neutron single-particle resonant states in ^{120}Sn with energies and widths $E-i\Gamma/2$ obtained by searching for the extrema of the Green's functions are listed, and these are compared with those obtained by exploring for the maximum of the DOS [72]. For most of the resonant states, exactly the same energies and widths are obtained while very small differences (within 0.2 keV) exist for others. Compared with the results obtained by comparing the DOSs for nucleons and free particles in Ref. [66], four wide resonant states ($2g_{7/2}$, $2g_{9/2}$, $2h_{11/2}$, and $1j_{13/2}$) are identified. Furthermore, the accuracy of the width for the narrow resonant state $1h_{9/2}$ is highly refined to be 1×10^{-8} MeV. All these results prove that the approach by probing the extremum of the Green's functions is as effective and reliable as that by exploring for the extremum of the DOS in identifying the resonant states, irrespective of whether the resonant state is wide or narrow. Moreover, compared with the approach by exploring for the extremum of the DOS, the approach by searching for the extremum of the Green's functions is easier, more direct, and less time-consuming. However, without the DOS, this approach cannot describe intuitively the structures of the single-particle spectrum for the bound and resonant states.

5 Summary and perspectives

Significant roles are played by the single-particle resonances in the structure of exotic nuclei. The Green's function method has been demonstrated to be one of the most effective approaches in searching for single-particle resonant states. In our recent work [72], by probing the extremum of the DOSs $n_\kappa(\varepsilon)$ defined in a finite space size $R_{\rm box}$, the Green's function method has been proven to be very reliable, regardless of whether the resonances are wide or narrow. In this work, another direct and effective approach by probing the extremum of the Green's functions is proposed to identify the resonant states.

Taking the same nucleus ^{120}Sn as an example, by searching for the poles or extrema of the Green's functions, we obtain almost the same energies and widths for the resonant states as obtained by exploring for the extremum of the DOS. In addition, the dependence of the Green's functions on the space size is checked and found to be very stable. Compared with the results obtained by comparing the DOSs for nucleons and free particles [66], four wide resonant states ($2g_{7/2}$, $2g_{9/2}$, $2h_{11/2}$, and $1j_{13/2}$) are identified, and the accuracy of the width of the narrow resonant state $1h_{9/2}$ is highly refined to 1×10^{-8} MeV. All these results prove that the approach by probing the extremum of the Green's functions has the same reliability and effectiveness as that by probing the extremum of the DOS to identify the resonant states, regardless of whether the resonant states are wide or narrow.

As is well known, both pairing correlations and the continuum play core roles in exotic nuclei. Therefore, studies on the possible effects of pairing on the resonant states are significant and very interesting. In the investigations with the continuum Skyrme HFB approach in Refs. [38, 39], the authors concluded that the pairing correlation can enhance the resonant energies and widths for all quasiparticle resonances, whether hole-like or particle-like. However, in Ref. [77], an opposite conclusion was obtained for the particle-like quasiparticle resonances studied with a fixed resonant energy. In the future, we will take the self-consistent relativistic continuum Hartree–Bogoliubov model with the Green's function method [71] to explore the possible effects of pairing on the resonant states. Moreover, we would like to apply the Green's function method to dynamic reactions and search for resonance structures, for which vast theoretical and experimental works have been performed [78, 79]. In Ref. [80],

Table 1 Neutron single-particle resonances nl_j in ^{120}Sn with energies and widths $E-i\Gamma/2$ obtained by probing the extrema of the Green's functions, compared with the results by exploring for the extremum of the DOS in our previous study [72]. The PK1 effective density functional was used. All quantities are in MeV

Positive parity	Green's function	DOS	Negative parity	Green's function	DOS
$2g_{7/2}$	$6.3585-i3.1053$	$6.3585-i3.1052$	$3p_{1/2}$	$0.0504-i0.0164$	$0.0504-i0.0164$
$2g_{9/2}$	$5.4428-i1.6948$	$5.4428-i1.6948$	$2f_{5/2}$	$0.8705-i0.0326$	$0.8705-i0.0325$
$1i_{11/2}$	$9.8544-i0.6413$	$9.8544-i0.6413$	$1h_{9/2}$	$0.2507-i4\times10^{-8}$	$0.2508-i4\times10^{-8}$
$1i_{13/2}$	$3.4686-i0.0025$	$3.4686-i0.0024$	$2h_{11/2}$	$10.5130-i6.7683$	$10.5130-i6.7681$
			$1j_{13/2}$	$18.1846-i3.1532$	$18.1846-i3.1531$
			$1j_{15/2}$	$12.8929-i0.5323$	$12.8929-i0.5322$

the complex molecular resonances in the $^{12}C+^{12}C$ fusion reaction were explored with the thick-target method.

Acknowledgements Helpful discussions with Prof. Z. P. Li are highly appreciated.

Author Contributions All authors contributed to the study conception and design. Material preparation, data collection, and analysis were performed by Ya-Tian Wang and Ting-Ting Sun. The first draft of the manuscript was written by Ya-Tian Wang and all authors commented on previous versions of the manuscript. All authors read and approved the final manuscript.

References

1. I. Tanihata, H. Hamagaki, O. Hashimoto et al., Measurements of interaction cross sections and nuclear radii in the light *p*-shell region. Phys. Rev. Lett. **55**, 2676 (1985). https://doi.org/10.1103/PhysRevLett.55.2676
2. N. Kobayashi, T. Nakamura, Y. Kondo et al., Observation of a *p*-wave one-neutron halo configuration in ^{37}Mg. Phys. Rev. Lett. **112**, 242501 (2014). https://doi.org/10.1103/PhysRevLett.112.242501
3. J. Meng, P. Ring, Giant halo at the neutron drip line. Phys. Rev. Lett. **80**, 460 (1998). https://doi.org/10.1103/PhysRevLett.80.460
4. J. Meng, H. Toki, J.Y. Zeng et al., Giant halo at the neutron drip line in Ca isotopes in relativistic continuum Hartree-Bogoliubov theory. Phys. Rev. C **65**, 041302 (2002). https://doi.org/10.1103/PhysRevC.65.041302
5. M. Grasso, S. Yoshida, N. Sandulescu et al., Giant neutron halos in the non-relativistic mean field approach. Phys. Rev. C **74**, 064317 (2006). https://doi.org/10.1103/PhysRevC.74.064317
6. S.-G. Zhou, J. Meng, P. Ring et al., Neutron halo in deformed nuclei. Phys. Rev. C **82**, 011301 (2010). https://doi.org/10.1103/PhysRevC.82.011301
7. L.L. Li, J. Meng, P. Ring et al., Deformed relativistic Hartree-Bogoliubov theory in continuum. Phys. Rev. C **85**, 024312 (2012a). https://doi.org/10.1103/PhysRevC.85.024312
8. X.X. Sun, J. Zhao, S.G. Zhou, Shrunken halo and quenched shell gap at $N = 16$ in ^{22}C: Inversion of *sd* states and deformation effects. Phys. Lett. B **785**, 530 (2018a). https://doi.org/10.1016/j.physletb.2018.08.071
9. J. Dobaczewski, W. Nazarewicz, T.R. Werner et al., Mean-field description of ground-state properties of drip-line nuclei: pairing and continuum effects. Phys. Rev. C **53**, 2809 (1996). https://doi.org/10.1103/PhysRevC.53.2809
10. J. Meng, Relativistic continuum Hartree-Bogoliubov theory with both zero range and finite range Gogny forces and their application. Nucl. Phys. A **635**, 3 (1998). https://doi.org/10.1103/PhysRevLett.55.267600
11. J. Humblet, B.W. Filippone, S.E. Koonin, Level matrix, ^{16}Nβ decay, and the $^{12}C(\alpha,\gamma)^{16}O$ reaction. Phys. Rev. C **44**, 2530 (1991). https://doi.org/10.1103/PhysRevLett.55.267601
12. J.R. Taylor, *Scattering Theory: The Quantum Theory on Non-relativistic Collisions* (Wiley, New York, 1972). https://doi.org/10.1063/1.3128052
13. L.G. Cao, Z.Y. Ma, Exploration of resonant continuum and giant resonance in the relativistic approach. Phys. Rev. C **66**, 024311 (2002). https://doi.org/10.1103/PhysRevC.66.024311
14. G.M. Hale, R.E. Brown, N. Jarmie, *S*-matrix and *R*-matrix determination of the low-energy ^{5}He and ^{5}Li resonance parameters. Phys. Rev. Lett. **59**, 763 (1987). https://doi.org/10.1103/PhysRevC.55.536
15. E.P. Wigner, L. Eisenbud, Higher angular momenta and long range interaction in resonance reactions. Phys. Rev. **72**, 29 (1947). https://doi.org/10.1103/PhysRev.72.29
16. B.N. Lu, E.G. Zhao, S.G. Zhou, Pseudospin symmetry in single particle resonant states. Phys. Rev. Lett. **109**, 072501 (2012). https://doi.org/10.1103/PhysRevLett.109.072501
17. B.N. Lu, E.G. Zhao, S.-G. Zhou, Pseudospin symmetry in single-particle resonances in spherical square wells. Phys. Rev. C **88**, 024323 (2013). https://doi.org/10.1103/PhysRevC.88.024323
18. Z.P. Li, J. Meng, Y. Zhang et al., Single-particle resonances in a deformed Dirac equation. Phys. Rev. C **81**, 034311 (2010a). https://doi.org/10.1103/PhysRevC.81.034311
19. Z.P. Li, Y. Zhang, D. Vretenar et al., Single-particle resonances in a deformed relativistic potential. Sci. China-Phys. Mech. Astron. **53**, 773 (2010b). https://doi.org/10.1007/s11433-010-0161-7
20. A.U. Hazi, H.S. Taylor, Stabilization method of calculating resonance energies: model problem. Phys. Rev. A **1**, 1109 (1970). https://doi.org/10.1103/PhysRevA.1.1109
21. K. Hagino, N. Van Giai, Structure of positive energy states in a deformed mean-field potential. Nucl. Phys. A **735**, 55 (2004). https://doi.org/10.1063/1.312805200
22. B. Gyarmati, A.T. Kruppa, Complex scaling in the description of nuclear resonances. Phys. Rev. C **34**, 95 (1986). https://doi.org/10.1063/1.312805201
23. A.T. Kruppa, P.H. Heenen, H. Flocard et al., Particle-unstable nuclei in the Hartree-Fock theory. Phys. Rev. Lett. **79**, 2217 (1997). https://doi.org/10.1103/PhysRevLett.79.2217
24. J.Y. Guo, X.Z. Fang, P. Jiao et al., Application of the complex scaling method in relativistic mean-field theory. Phys. Rev. C **82**, 034318 (2010). https://doi.org/10.1103/PhysRevC.82.034318
25. S.Y. Wang, Z.L. Zhu, Z.M. Niu, Influence of the Coulomb exchange term on nuclear single-proton resonances. Nucl. Sci. Tech. **27**, 122 (2016). https://doi.org/10.1007/s41365-016-0125-3
26. S.S. Zhang, J. Meng, S.G. Zhou et al., Analytic continuation of single-particle resonance energy and wave function in relativistic mean field theory. Phys. Rev. C **70**, 034308 (2004). https://doi.org/10.1103/PhysRevC.70.034308
27. S.S. Zhang, M.S. Smith, Z.S. Kang et al., Microscopic self-consistent study of neon halos with resonant contributions. Phys. Lett. B **730**, 30 (2014). https://doi.org/10.1016/j.physletb.2014.01.023
28. G. Hagen, J.S. Vaagen, Study of resonant structures in a deformed mean field using the contour deformation method in the momentum space. Phys. Rev. C **73**, 034321 (2006). https://doi.org/10.1063/1.312805277
29. N. Li, M. Shi, J.-Y. Guo et al., Probing resonances of the Dirac equation with complex momentum representation. Phys. Rev. Lett. **117**, 062502 (2016). https://doi.org/10.1103/PhysRevLett.117.062502
30. M. Shi, X.X. Shi, Z.M. Niu et al., Relativistic extension of the complex scaled Green's function method for resonances in deformed nuclei. Eur. Phys. J. A **53**, 40 (2017). https://doi.org/10.1140/epja/i2017-12241-6
31. E. Tamura, Relativistic single-site Green function for general potentials. Phys. Rev. B **45**, 3271 (1992). https://doi.org/10.1103/PhysRevC.66.024311000
32. D.L. Foulis, Partial-wave Green-function expansions for general potentials. Phys. Rev. A **70**, 022706 (2004). https://doi.org/10.1103/PhysRevC.66.024311101
33. A. Horri, R. Faez, Full-quantum simulation of graphene self-switching diodes. Chin. Phys. Lett. **36**, 067202 (2019). https://doi.org/10.1088/0256-307x/36/6/067202
34. S.-Q. Jia, Finite volume time domain with the Green function method for electromagnetic scattering in Schwarzschild

spacetime. Chin. Phys. Lett. **36**, 010401 (2019). https://doi.org/10.1088/0256-307x/36/1/010401
35. Y. Zhang, M. Matsuo, J. Meng, Persistent contribution of unbound quasiparticles to the pair correlation in the continuum Skyrme-Hartree-Fock-Bogoliubov approach. Phys. Rev. C **83**, 054301 (2011). https://doi.org/10.1103/PhysRevC.66.0243112
36. Y. Zhang, M. Matsuo, J. Meng, Pair correlation of giant halo nuclei in continuum Skyrme-Hartree-Fock-Bogoliubov theory. Phys. Rev. C **86**, 054318 (2012). https://doi.org/10.1103/PhysRevC.66.0243113
37. X.Y. Qu, Y. Zhang, Canonical states in continuum Skyrme Hartree-Fock-Bogoliubov theory with Green's function method. Phys. Rev. C **99**, 014314 (2019a). https://doi.org/10.1103/PhysRevC.66.0243114
38. X.Y. Qu, Y. Zhang, Effects of mean-field and pairing correlations on the Bogoliubov quasiparticle resonance. Sci. China-Phys. Mech. Astron. **62**, 112012 (2019b). https://doi.org/10.1103/PhysRevC.66.0243115
39. Y. Zhang, X.Y. Qu, Effects of pairing correlation on the quasiparticle resonance in neutron-rich Ca isotopes. Phys. Rev. C **102**, 054312 (2020b). https://doi.org/10.1103/PhysRevC.66.0243116
40. T.T. Sun, Z.X. Liu, L. Qian et al., Continuum Skyrme-Hartree-Fock-Bogoliubov theory with Green's function method for odd$A$ nuclei. Phys. Rev. C **99**, 054316 (2019a). https://doi.org/10.1103/PhysRevC.99.054316
41. S.T. Belyaev, A.V. Smirnov, S.V. Tolokonnikov et al., Pairing in atomic nuclei in the coordinate representation. Sov. J. Nucl. Phys. **45**, 783 (1987)
42. M. Matsuo, Continuum linear response in coordinate space Hartree-Fock-Bogoliubov formalism for collective excitations in drip-line nuclei. Nucl. Phys. A **696**, 371 (2001). https://doi.org/10.1103/PhysRevC.66.0243118
43. M. Matsuo, Collective excitations and pairing effects in drip-line nuclei: continuum RPA in coordinate-space HFB Prog. Theor. Phys. Suppl. **146**, 110 (2002). https://doi.org/10.1103/PhysRevC.66.0243119
44. M. Matsuo, K. Mizuyama, Y. Serizawa, Di-neutron correlation and soft dipole excitation in medium-mass neutron-rich nuclei near the drip line. Phys. Rev. C **71**, 064326 (2005). https://doi.org/10.1103/PhysRevC.55.53600
45. K. Mizuyama, M. Matsuo, Y. Serizawa, Continuum quasiparticle linear response theory using the Skyrme functional for multipole responses of exotic nuclei. Phys. Rev. C **79**, 024313 (2009). https://doi.org/10.1103/PhysRevC.55.53611
46. M. Matsuo, Y. Serizawa, Surface-enhanced pair transfer amplitude in the quadrupole states of neutron-rich Sn isotopes. Phys. Rev. C **82**, 024318 (2010). https://doi.org/10.1103/PhysRevC.55.53622
47. H. Shimoyama, M. Matsuo, Anomalous pairing vibration in neutron-rich Sn isotopes beyond the $N = 82$ magic number. Phys. Rev. C **84**, 044317 (2011). https://doi.org/10.1103/PhysRevC.55.53633
48. H. Shimoyama, M. Matsuo, Di-neutron correlation in monopole two-neutron transfer modes in the Sn isotope chain. Phys. Rev. C **88**, 054308 (2013). https://doi.org/10.1103/PhysRevC.55.53644
49. M. Matsuo, Continuous quasiparticle random-phase approximation for astrophysical direct neutron capture reactions on neutron-rich nuclei. Phys. Rev. C **91**, 034604 (2015). https://doi.org/10.1103/PhysRevC.55.53655
50. J. Meng, H. Toki, S.G. Zhou et al., Relativistic continuum Hartree Bogoliubov theory for ground-state properties of exotic nuclei. Prog. Part. Nucl. Phys. **57**, 470 (2006b). https://doi.org/10.1016/j.ppnp.2005.06.001
51. P. Ring, Relativistic mean field theory in finite nuclei. Prog. Part. Nucl. Phys. **37**, 193 (1996). https://doi.org/10.1103/PhysRevC.55.53677
52. D. Vretenar, A.V. Afanasjev, G.A. Lalazissis et al., Relativistic Hartree-Bogoliubov theory: static and dynamic aspects of exotic nuclear structure. Phys. Rep. **409**, 101 (2005). https://doi.org/10.1103/PhysRevC.55.53688
53. A. Sobiczewski, K. Pomorski, Description of structure and properties of superheavy nuclei. Prog. Part. Nucl. Phys. **58**, 292 (2007). https://doi.org/10.1103/PhysRevC.55.53699
54. N. Wang, E.G. Zhao, W. Scheid et al., Theoretical study of the synthesis of superheavy nuclei with $Z = 119$ and 120 in heavy-ion reactions with trans-uranium targets. Phys. Rev. C **85**, 041601 (2012). https://doi.org/10.1103/PhysRevC.85.041601
55. W. Zhang, Y.F. Niu, Shape transition with temperature of pear-shaped nuclei in covariant density functional theory. Phys. Rev. C **96**, 054308 (2017a). https://doi.org/10.1103/PhysRev.72.2911
56. H.Z. Liang, J. Meng, S.G. Zhou, Hidden pseudospin and spin symmetries and their origins in atomic nuclei. Phys. Rep. **570**, 1 (2015). https://doi.org/10.1016/j.physrep.2014.12.005
57. W.L. Lu, Z.X. Liu, S.H. Ren et al., (Pseudo) Spin symmetry in the single-neutron spectrum of Λ hypernuclei. J. Phys. G Nucl. Part. Phys. **44**, 125104 (2017). https://doi.org/10.1088/1361-6471/aa8e2d
58. T.T. Sun, W.L. Lu, S.S. Zhang, Spin and pseudospin symmetries in the single-Λ spectrum. Phys. Rev. C **96**, 044312 (2017). https://doi.org/10.1103/PhysRevC.96.044312
59. B.N. Lu, E.G. Zhao, S.-G. Zhou, The quadrupole deformation (β, γ) of light Λ hypernuclei in a constrained relativistic mean field model: the shape evolution and shape polarization effect of the Λ hyperon. Phys. Rev. C **84**, 014328 (2011). https://doi.org/10.1103/PhysRevC.84.014328
60. T.T. Sun, E. Hiyama, H. Sagawa et al., Mean-field approaches for Ξ^- hypernuclei and current experimental data. Phys. Rev. C **94**, 064319 (2016a). https://doi.org/10.1103/PhysRevC.94.064319
61. Z.X. Liu, C.J. Xia, W.L. Lu et al., Relativistic mean-field approach for Λ, Ξ, and Σ hypernuclei. Phys. Rev. C **98**, 024316 (2018). https://doi.org/10.1103/PhysRevC.98.024316
62. B.J. Cai, L.W. Chen, Constraints on the skewness coefficient of the symmetric nuclear matter within the nonlinear relativistic mean field model. Nucl. Sci. Tech. **28**, 185 (2017). https://doi.org/10.1007/s41365-017-0329-1
63. T.T. Sun, C.J. Xia, S.S. Zhang et al., Massive neutron stars and hypernuclei in relativistic mean field models. Chin. Phys. C **42**, 025101 (2018b). https://doi.org/10.1088/1674-1137/42/2/025101
64. J. Daoutidis, P. Ring, Continuum random-phase approximation for relativistic point coupling models. Phys. Rev. C **80**, 024309 (2009). https://doi.org/10.1103/PhysRevLett.109.072501 0
65. D. Yang, L.G. Cao, Y. Tian et al., Importance of self-consistency in relativistic continuum random-phase approximation calculations. Phys. Rev. C **82**, 054305 (2010). https://doi.org/10.1103/PhysRevC.82.054305
66. T.T. Sun, S.Q. Zhang, Y. Zhang et al., Green's function method for single-particle resonant states in relativistic mean-field theory. Phys. Rev. C **90**, 054321 (2014). https://doi.org/10.1103/PhysRevC.90.054321
67. T.T. Sun, Z.M. Niu, S.Q. Zhang, Single-proton resonant states and isospin dependence were investigated by Green's function relativistic mean field theory. J. Phys. G: Nucl. Part. Phys. **43**, 045107 (2016b). https://doi.org/10.1088/0954-3899/43/4/045107
68. S.H. Ren, T.T. Sun, W. Zhang, Green's function relativistic mean field theory for Λ hypernuclei. Phys. Rev. C **95**, 054318 (2017). https://doi.org/10.1103/PhysRevC.95.054318
69. T.T. Sun, L. Qian, C. Chen et al., Green's function method for single-particle resonances in a deformed Dirac equation. Phys. Rev. C **101**, 014321 (2020). https://doi.org/10.1103/PhysRevC.101.014321
70. T.T. Sun, W.L. Lu, L. Qian et al., Green's function method for spin and pseudospin symmetries in single-particle resonant states.

Phys. Rev. C **99**, 034310 (2019b). https://doi.org/10.1103/PhysRevC.99.034310
71. T.T. Sun, Green's function method in covariant density functional theory. Sci. Sin. Phys. Mech. Astron. **46**, 12006 (2016). https://doi.org/10.1360/SSPMA2015-00371 (**in Chinese**)
72. C. Chen, Z.P. Li, Y.X. Li et al., Single-particle resonant states with Green's function method. Chin. Phys. C **44**, 084105 (2020). https://doi.org/10.1088/1674-1137/44/8/084105
73. J.Y. Fang, S.W. Chen, T.H. Heng, Solution to the Dirac equation using the finite difference method. Nucl. Sci. Tech. **31**, 15 (2020). https://doi.org/10.1007/s41365-020-0728-6
74. Y.K. Gambhir, P. Ring, A. Thimet, Relativistic mean field theory for finite nuclei. Phys. Rev. C **68**, 132 (1990). https://doi.org/10.1016/0003-4916(90)90330-Q
75. S.G. Zhou, J. Meng, P. Ring, Spherical relativistic Hartree theory in a Woods-Saxon basis. Phys. Rev. C **68**, 034323 (2003). https://doi.org/10.1103/PhysRevC.68.034323
76. P.W. Zhao, Z.P. Li, J.M. Yao et al., New parametrization for the nuclear covariant energy density functional with a point-coupling interaction. Phys. Rev. C **82**, 054319 (2010). https://doi.org/10.1103/PhysRevC.82.054319
77. Y. Kobayashi, M. Matsuo, Effects of pairing correlation on low-lying quasiparticle resonance in neutron drip-line nuclei. Prog. Theor. Exp. Phys. **2016**, 013D01 (2016). https://doi.org/10.1093/ptep/ptv175
78. W.J. Li, Y.G. Ma, G.Q. Zhang et al., Yield ratio of neutrons to protons in ^{12}C(d, n)^{13}N and ^{12}C(d, p)^{13}C from 0.6 MeV to 3 MeV. Nucl. Sci. Tech. **30**, 180 (2019). https://doi.org/10.1007/s41365-019-0705-0
79. H.R. Guo, Y.L. Han, C.H. Cai, Theoretical calculation and evaluation of n+^{240,242,244}Pu reactions. Nucl. Sci. Tech. **30**, 13 (2019). https://doi.org/10.1007/s41365-018-0533-7
80. X.D. Tang, S.B. Ma, X. Fang et al., An efficient method for mapping the ^{12}C+^{12}C molecular resonances at low energies. Nucl. Sci. Tech. **30**, 126 (2019). https://doi.org/10.1007/s41365-019-0652-9